Kim and Kim *Biochar (2026)8:73*
https://doi.org/10.1007/s42773-026-00584-1

Biochar

ORIGINAL RESEARCH Open Access

Highly porous biochar from spent coffee ground for fully green thermal insulating composites with thermal conductivity of 0.04 W m^{-1} K^{-1}

Sung Jin Kim[1] and Seong Yun Kim[1*]

Abstract

Biomass materials offer the advantages of low cost, abundant availability, and renewability, making them sustainable and environmentally friendly alternatives to petroleum-based thermal insulation materials. Spent coffee ground (SCG), a type of biomass generated after brewing coffee, has been used as a filler for thermal insulation composites. However, developing SCG-based composites with superior thermal insulation performance remains a significant challenge due to the low porosity of SCG. Herein, a highly porous SCG biochar (SB) was fabricated by a simple carbonization process optimized for temperature and atmosphere. SB-based thermal insulation polymer composites were designed and fabricated for the first time, employing the SB as the filler and biodegradable ethyl cellulose (EC) as the matrix. Meanwhile, the SB was pre-mixed with environmentally friendly solvents (water, ethanol, and propylene glycol) selected based on the chemical interaction within the material system to prevent the impregnation of SB pores with the EC. The chemical and morphological properties of the SB were discussed in terms of their influence on the thermal insulation properties of the fabricated composite. The thermal conductivity and heat transfer mechanism of the SB-based composites were systematically verified using steady-state heat transfer theory. The biodegradable SB-based composite demonstrated outstanding thermal insulation property (0.04 W m^{-1} K^{-1}) comparable to commercial expanded polystyrene. More importantly, the thermal insulation composites developed in this work consisted of environmentally friendly and sustainable materials, free from hazardous or toxic substances. These thermally insulating and biodegradable SB-based polymer composites are expected to be widely utilized in various thermal insulation applications.

Highlights

- Fully green SB-based composites exhibited excellent insulation performance (0.04 W m^{-1} K^{-1}), comparable to that of EPS.
- The effect of SB structure on thermal conductivity was validated by finite element simulation based on Fourier's law.
- Biodegradable SB-based thermal insulators contribute to the circular economy by upcycling large-scale coffee waste.

Keywords Spent coffee ground, Biochar, Green material, Thermal insulation composite, Biodegradability

*Correspondence:
Seong Yun Kim
sykim82@jbnu.ac.kr

Springer

Graphical Abstract

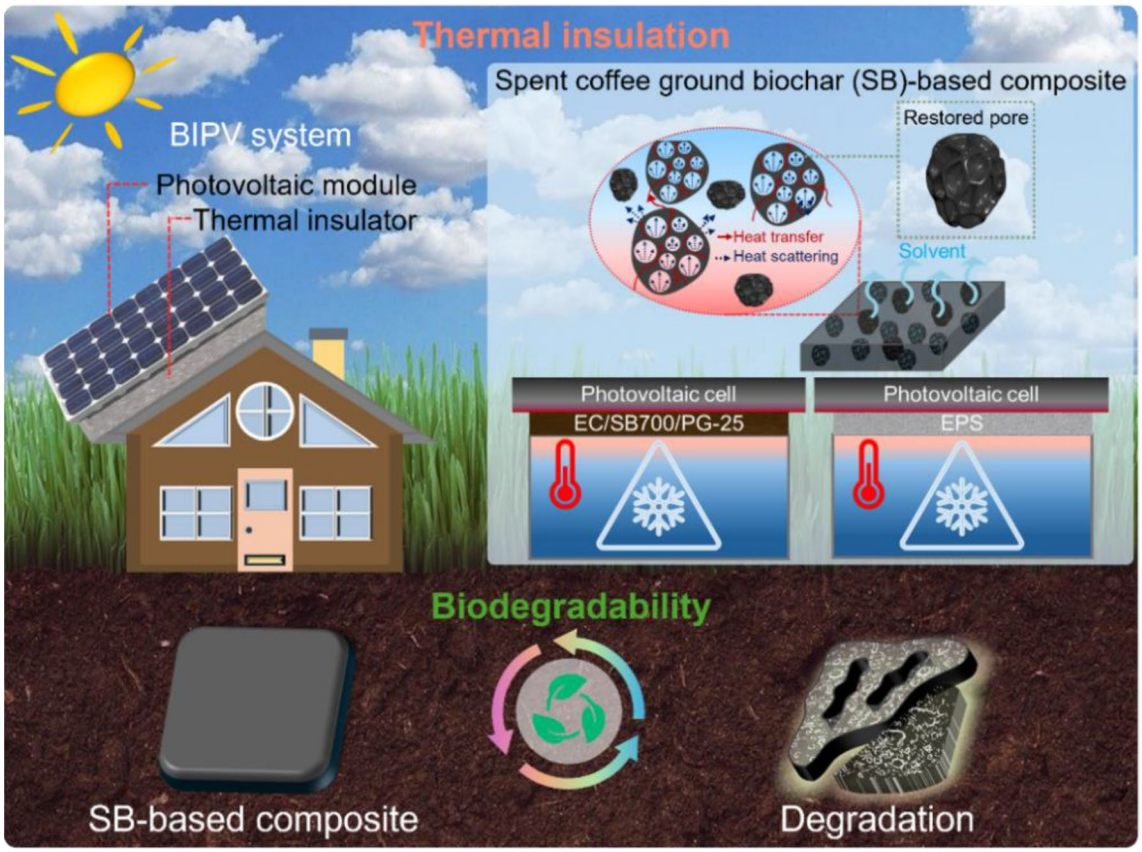

1 Introduction

Thermally insulating materials are used to improve energy efficiency and are applied in areas where precise temperature regulation is essential (Zhang et al. 2024a; Zhang et al. 2023). The demand for thermal insulation is increasing exponentially due to the wide range of potential applications in the building, transportation, and food-packaging industries (Zhang et al. 2023; Chen et al. 2023). Thermal insulation is a crucial element of global efforts to reduce energy demand and carbon emissions (De Rosa and Bianco 2023). Commonly used petroleum-based thermal insulation materials (e.g., expanded polystyrene (EPS) and polyurethane foam) are harmful to both humans and the environment due to improper disposal methods and the finite availability of fossil fuels (Zhang et al. 2023; MacLeod et al. 2021). Despite these constraints, petroleum-based thermal insulation materials are favored due to their low cost, low thermal conductivity, and versatility (Mort et al. 2021; Varamesh et al. 2024). However, recent regulations restricting the use of styrene in Europe have prompted an urgent need to replace styrene-based thermal insulation materials and develop more environmentally friendly alternatives (Desole et al. 2024).

As the green transition accelerates, increasing attention has been directed toward thermal insulation materials that prioritize sustainability, environmental compatibility, and renewability (Tan et al. 2023). Several studies have reported green thermal insulation composites developed from a wide range of bio-based sources, such as cork (Qi et al. 2024), date palm wood (Abu-Jdayil et al. 2021; AlMallahi et al. 2024), banana peel (Di Canto et al. 2023), mycelium (Zhang et al. 2023), oil palm trunk (Mawardi et al. 2022), wheat husk (Hýsek et al. 2018; Muthuraj et al. 2019), hemp shiv (Viel et al. 2019), corn cob (Viel et al. 2019), and sunflower stalk (Mati-Baouche et al. 2014). Abu-Jdayil et al. reported a polylactic acid (PLA)-based biodegradable thermal insulation composite

incorporating date palm wood powder for building applications, which exhibited a thermal conductivity of about 0.07 W m^{-1} K^{-1}. Zhang et al. (2023) developed a mycelium-based thermal insulator using porous sawdust as a substrate, which exhibited superior thermal insulation performance (0.04 W m^{-1} K^{-1}) comparable to that of EPS. Qi et al. (2024) fabricated a rigid polyurethane foam with 24 wt% cork, reaching a thermal conductivity of approximately 0.04 W m^{-1} K^{-1}. Although green thermal insulation composites provide significant environmental benefits, they still show limited performance and environmental challenges. Fabrication processes such as fungal cultivation are inherently complex, requiring considerable time and energy. Meanwhile, biomass-based polymeric thermal insulators offer excellent thermal insulation performance but pose environmental concerns at the end of their life cycle. Moreover, thermal insulation composites utilizing biochar derived from various biomass sources have been investigated. Zhang et al. (2025) reported a gypsum plaster composite incorporating biochar produced from tree-branch wood waste, exhibiting a thermal conductivity of approximately 0.27 W m^{-1} K^{-1}. A sugarcane bagasse biochar/cement composite achieved about 0.23 W m^{-1} K^{-1} (Rodier et al. 2019), and mortars containing biochar derived from oilseed rape and mixed softwood exhibited around 0.70 W m^{-1} K^{-1} (Park et al. 2021). However, these biochar-based inorganic composites suffer from clear performance limitations and environmental issues, such as poor biodegradability and the emission of hazardous substances during disposal (e.g., hydrogen sulfide gas (Xu et al. 2011) and heavy metal (Dell'Orso et al. 2012)). In addition, Kim et al. (2025) developed PLA composites incorporating orange-peel biochar coated with calcium and alginate through an additional complex process, achieving a thermal conductivity of 0.08 W m^{-1} K^{-1}. Overall, the performance and environmental drawbacks of existing green composites underscore the need for developing more sustainable thermal insulation materials.

Coffee, one of the most consumed beverages worldwide, is the second most traded product after oil (Li et al. 2024; García-García et al. 2015). Approximately 90% of coffee beans are wasted as spent coffee ground (SCG), generating about 8 million tons annually (Martinez et al. 2021; Shi et al. 2023). SCG mainly consists of cellulose, hemicellulose, and lignin, along with proteins, lipids, and small amounts of ash, phenolic compounds, caffeine, and tannins (McNutt and He 2019). SCG exhibits a high C/N ratio, high phenolic content, and strong acidity, making it unsuitable for composting. In contrast, biochar obtained from the pyrolysis of SCG, in which most volatile and harmful components are removed, possesses a porous carbon structure that is environmentally more beneficial. Although SCG has a high utilization value as biomass due to its composition, it is generally disposed of by landfilling or incineration, which adversely affects the environment (Li et al. 2024; García-García et al. 2015; Martinez et al. 2021; Shi et al. 2023; Seo et al. 2023; Kim et al. 2020). According to the British recycling company Bio-bean, reusing SCG could reduce carbon dioxide emissions from landfills by approximately 80% (Woo et al. 2021). Moreover, high-temperature incineration (> 1000 °C), adopted due to limited landfill capacity, not only contributes to air pollution but is also inefficient in terms of energy consumption (Seo et al. 2023; Li et al. 2023; Kataya et al. 2023). Accordingly, recycling or upcycling SCG into high-value-added materials (e.g., biochar, activated carbon, fertilizers, and CO_2 adsorbents) can reduce energy consumption and disposal costs while contributing to a sustainable circular economy (Li et al. 2024; García-García et al. 2015; Martinez et al. 2021; Shi et al. 2023; Seo et al. 2023; Kim et al. 2020; Woo et al. 2021). Attempts to recycle SCG as thermally insulating materials by utilizing its porous structure have been reported (Lachheb et al. 2019). However, SCG has a low porosity (approximately ~ 40%) (Kim et al. 2024), which may limit its thermal insulation efficiency. SCG biochar (SB), derived from the carbonization of SCG, exhibits a highly porous structure (~ 70%) (Kim et al. 2024). SB can be produced at lower temperatures than incineration, thereby reducing energy consumption and providing a sustainable and eco-friendly alternative to the conventional disposal of SCG (Zhou et al. 2022). Due to its high porosity, SB can serve as a filler for thermal insulation composites; however, limited studies have investigated this potential.

To maximize the thermal insulation properties of polymer composites with a porous filler, it is important to prevent the pores of the filler from being impregnated with the polymer matrix during fabrication (Boonrawd et al. 2022; Cho et al. 2019; Kim et al. 2018, 2015; Lee et al. 2019; Zhang et al. 2024b). An intact porous structure within the fillers is a dominant factor in achieving low thermal conductivity. Pore restoration and preservation methods to prevent impregnation of the filler pores with the matrix have been proposed (Boonrawd et al. 2022; Cho et al. 2019; Kim et al. 2015; Lee et al. 2019; Zhang et al. 2024b). In the pore restoration method, a solvent was pre-mixed with the porous filler to prevent impregnation of the polymer matrix, and the pores were subsequently restored by evaporation and diffusion of the solvent. Boonrawd et al. (2022) reported that premixing silica aerogel with a low-surface-energy organic solvent (n-hexane) enabled the restoration of its nanoporous structure upon solvent evaporation, resulting in a silica aerogel/natural rubber composite with a thermal conductivity of 0.06 W m^{-1} K^{-1}. In the pore preservation

method, a hydrophobic filler was applied to a hydrophilic polymer matrix to prevent filler pore impregnation by exploiting the affinity difference between the two materials. Zhang et al. (2024b) fabricated silica aerogel/poly(vinyl alcohol) (PVA) composites containing over 74 vol% silica aerogel using a hydrophilic PVA aqueous binder, which exhibited a low thermal conductivity of 0.03 W m^{-1} K^{-1} due to the preserved nanopore of the silica aerogel. The pore restoration method has a broader applicability compared to the limited scope of the pore preservation method. However, the interactions between the solvent, filler, and matrix must be taken into account when selecting the optimal solvent for the pore restoration method.

Herein, we propose a novel approach to the fabrication of environmentally friendly thermal insulation composites with an SB filler. Naturally derived ethyl cellulose (EC) was adopted as the matrix for SB-based thermal insulation composites (Oprea and Voicu 2020), imparting biodegradability. The chemical and morphological properties of the SB according to carbonization temperature and atmosphere determined the thermal insulation performance of SB-based composites. Based on the interaction between SB and EC, environmentally friendly solvents (water, ethanol (EtOH), and propylene glycol (PG)) for pore restoration were selected (Shakeel et al. 2014), and the solvent type and content were optimized. An in-depth theoretical analysis based on finite element simulations using COMSOL Multiphysics was performed to elucidate the heat transfer mechanism of SB-based composites, and the effect of SB on their thermal conductivity was systematically investigated. Finally, the biodegradable SB-based composite demonstrated thermal insulation performance comparable to commercial EPS, highlighting its practical potential as a sustainable and environmentally friendly thermal insulator.

2 Materials and methods

2.1 Materials

SCG from the discarded coffee capsules was utilized as a raw material for thermal insulation filler. After washing with water, the SCG was oven-dried at 80 °C for 1 week. EC, a naturally derived polymer based on cellulose, was used as a raw material without chemical treatment (Oprea and Voicu 2020). Water, EtOH, and PG were used as solvents. EPS was used to compare the thermal insulation performance of the composites, and its properties are presented in Table S1 and Fig. S1. Specific information on the materials can be found in Section S1 of the Supplementary Information.

2.2 Fabrication of SB

Carbonization of SCG was performed using a tube furnace under an ambient atmosphere without gas flow. 3 g of SCG placed in an alumina mold was carbonized at different temperatures (500, 700, and 900 °C) for 1 h at a heating rate of 5 °C min^{-1}, as shown in Fig. 1 and Table S2 (the "x" of the sample label SBx denotes the applied carbonization temperature). To investigate the effect of the carbonization atmosphere on the filler, NSB700 was prepared at 700 °C under a nitrogen atmosphere with a flow rate of 200 mL min^{-1}, following the same procedure.

2.3 Fabrication of SB-based composites

As summarized in Table S3, EC and SB were weighed according to the target content. SB was pre-mixed with PG (2 g of PG per 1 g of SB) using a Thinky mixer. The pre-treated SB and EC were mixed at 200 rpm for 2 min. The powder mixture was placed in a 25×25 mm mold and compressed at 150 °C and 15 MPa for 10 min using a heating press. The residual solvent in the composite was then removed in a vacuum oven at 80 °C for 1 h. The composites applied to the pore restoration method with PG were labeled EC/X/PG-Y (X and Y represent the type and weight fraction of the filler, respectively). Control samples (Table S4) were prepared by the same method using different types of solvents. Details of the sample characterization are presented in Section S2.

2.4 Quantitative evaluation of solvent affinity

The Hansen solubility parameter (HSP) was used to quantitatively evaluate the solubility and chemical affinity between the substances (Hansen 1967). The R_a, defined as the HSP distance, was calculated to assess the solubility between the matrix and the solvent according to the following equation (Li et al. 2022):

$$R_a = \left\{4(\delta_{d1} - \delta_{d2})^2 + \left(\delta_{p1} - \delta_{p2}\right)^2 + (\delta_{h1} - \delta_{h2})^2\right\}^{1/2} \quad (1)$$

where δ_d, δ_p, and δ_h are the dispersion, polar, and hydrogen-bonding force terms of HSP, and the subscripts 1 and 2 denote two different materials. The relative energy difference (RED) is calculated according to Li et al. (2022):

$$RED = R_a/R_0 \quad (2)$$

where R_0 is the radius of interaction, defined as the maximum distance used to determine a good solvent (Li et al. 2022; Brown et al. 2024). The wettability of the SB filler with the solvent was evaluated using the sessile drop method with 5 μL of the solvent by a contact angle goniometer.

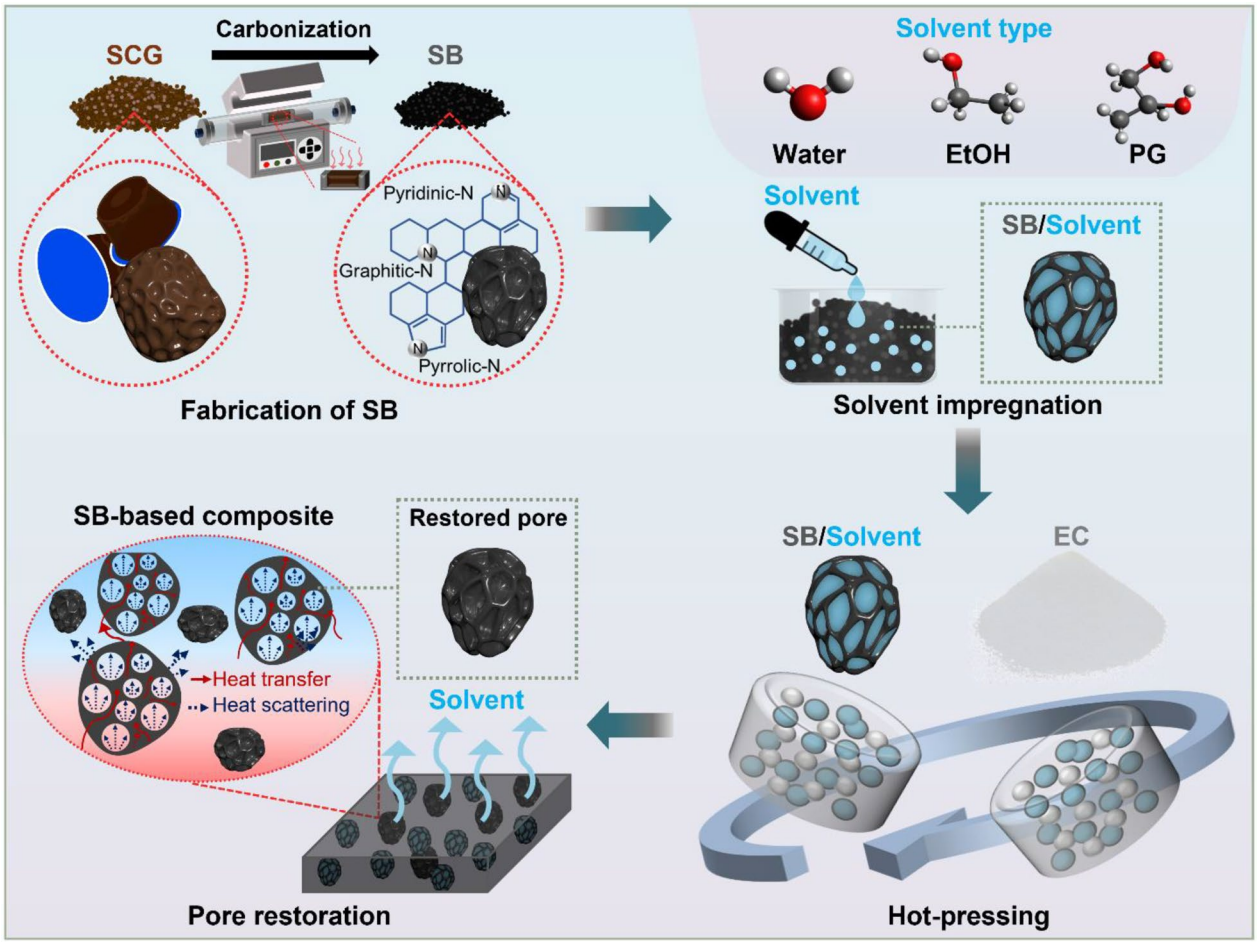

Fig. 1 Schematic illustration of the fabrication for SB and SB-based composites with pore restoration

2.5 Theoretical simulation

A finite element method (FEM) simulation using COMSOL software (COMSOL Inc., Burlington, MA, USA) was performed to theoretically evaluate the thermal conductivity of SB-based composites. The objective was to identify the factors influencing the heat transfer mechanism in the composites and to explore the effect of SB on their thermal conductivity. A parametric study on interfacial thermal resistance (ITR) between the SB and the EC matrix was also conducted.

2.5.1 Simulation framework

A theoretical simulation for a 3D geometry was conducted using the steady-state heat transfer mode. Detailed information on the governing equations used in the FEM simulations is provided in Section S3. The simulation model and boundary conditions are shown in Fig. 2a. The geometries of SB-based composites were built according to the volume fraction calculated from the apparent density. A two-component unit cell was used to simplify the geometric complexity caused by the numerous fillers dispersed in the matrix. The porous filler was modeled with a spherical geometry, and the material properties of SB and EC were set as shown in Table S5. The top and bottom surfaces of the geometry were assigned temperatures of 20 °C and 70 °C, respectively. All other surfaces were insulated, allowing heat to flow only in the z direction. To consider the interface effect of SB encapsulated by EC, it was assumed that SB was coated with a thin interfacial layer. In the ITR, defined as $10^{-\alpha}$, α was the model parameter at the SB interface. All simulation models adopted the same boundary conditions and procedures. The simulated thermal conductivity (λ) of the composites was calculated by the following equation (Xu et al. 2020):

$$\lambda = \frac{\Phi d}{\triangle T} \tag{3}$$

where Φ, d, and $\triangle T$ are heat flux density along the z direction, thickness in the z direction, and the temperature difference between the upper and lower surfaces, respectively. The results of the parametric simulation for SB700- and SB900-based composites are shown in Fig. 2b–d. The simulated thermal conductivity decreased as α decreased (Fig. 2b, c). These simulation results revealed that the smaller the α, the greater the influence on the interface effect.

2.6 Biodegradability test

Cellulose-based polymers were degraded by the hydrolytic actions of the cellulase enzyme (Xu et al. 2023). To evaluate the biodegradability of SB-based thermal insulation composites, a degradation test was performed using a cellulase enzyme produced by cellulolytic bacteria and fungi. A solution was prepared by adding cellulase to a 0.1 M acetate buffer at pH 5. Samples immersed in the solution were incubated at 50 °C for 3 weeks. After enzyme treatment, the samples were rinsed and dried at 80 °C for 24 h. Biodegradability was evaluated based on weight loss, as follows:

$$Weightloss(\%) = \left(\frac{Initialweight - Finalweight}{Initialweight}\right) \times 100 \quad (4)$$

3 Results and discussion

3.1 Structural characterization of SB

The variation in the chemical structure of the SCG according to carbonization was identified by FT-IR and XPS spectra. The FT-IR spectra of SCG and SB are presented in Fig. 3a. The broad peak at 3344 cm^{-1} for SCG is related to O–H stretching of the hydroxyl group in cellulose, hemicellulose, and lignin (Batista et al. 2020). Aliphatic C–H stretching (2925 and 2855 cm^{-1}), C=O stretching (1739 cm^{-1}), and aliphatic C=C bending (1631 cm^{-1}) were also evident (Batista et al. 2020; Lee et al. 2022; Bejenari et al. 2021; Liu and Huang 2018). Most of the functional groups in SCG, except for N–H (1530 cm^{-1}) and C–O stretching (1130–995 cm^{-1}) peaks, were eliminated by carbonization (Batista et al. 2020; Liu and Huang 2018). The removal of the functional groups in SB increased with the high carbonization temperature and showed the highest level of elimination in SB900. Thus, it was identified that the carbonization temperature was the major factor inducing chemical structural change. The deconvoluted XPS spectra of the SB are represented in Fig. 3b–d. The C1s spectra were separated into C–O (288.9–288.5 eV), C–N (286.5–286.3 eV), C–C (285.5–285.3 eV), and C=C (284.7–284.6 eV) peaks (Kim et al. 2024; Mengesha et al. 2022). The O1s spectra were deconvoluted into C–O (534.4–533.2 and 532.6–531.8 eV) and C–O–C (533.2–532.9 eV) peaks (Kim et al. 2024; Chan et al. 2022). These deconvoluted peaks in the C1s and O1s were typically observed in the biochar (Kim et al. 2024; Ghorbani et al. 2024). In the N1s spectra, the peaks were divided into graphitic N (401.1 eV), pyrrolic N (399.8–399.6 eV), and pyridinic N (398.2–397.6 eV) (Kim et al. 2024; Mengesha et al. 2022; Oh et al. 2019). During heat treatment, nitrogen-containing SCG could be converted to the nitrogen-doped carbon structure after dehydration, condensation, and aromatization (Mengesha et al. 2022; Wan et al. 2020). The nitrogen atoms in SCG were successfully incorporated into the carbon units, generating a nitrogen-doped carbon structure in the prepared SB. The peak of graphitic N, which is an sp^2 hybridized graphitic structure with nitrogen, was observed only in SB900 (Wan et al. 2020). These results indicated that the carbonization temperature influenced not only the chemical structure but also the formation of nitrogen-doped graphitic structure.

The XRD spectra of SCG and SB are represented in Fig. 3e. In the SCG, peaks at 16° and 20° indicate the (110) and (200) crystal planes of cellulose, respectively (Lee et al. 2022). After carbonization, the crystal structure transformed, and peaks at 23° and 43° emerged. The peaks at 24° and 43° were the (002) and (100) crystal planes of the graphitic carbon, indicating that SB was composed of sp^2 hybridized carbon structures (Andrade et al. 2020). The (100) crystal plane intensity increased with increasing carbonization temperature, indicating enhanced graphitic structure development at higher temperatures. Raman analysis was conducted to verify the development of the graphitic structure (Fig. 3f). In carbonaceous materials, the D (1350 cm^{-1}) and G (1580 cm^{-1}) bands generally appear, corresponding to defects and graphitic structures, respectively (Kim et al. 2024; Mengesha et al. 2022). The intensity ratio of the D and G bands (I_D/I_G) can be used to evaluate the degree of graphitic structure development (Kim et al. 2024; Mengesha et al. 2022). As the carbonization temperature increased, the I_D/I_G ratio decreased from 1.04 to 0.96, indicating enhanced graphitic structures. Therefore, the carbonization temperature was a major factor in the formation of the graphitic structure.

Morphological data of the SCG and SB are illustrated in Fig. 4. The quantitative pore characteristics are summarized in Table S2. The surface structure of SB was transformed into open pores by carbonization (Fig. 4a–h). The porous structure became evident as the carbonization temperature increased from 500 °C to 700 °C. As shown in Fig. 4i, the total porosities of SCG, SB500, SB700, and SB900 were 46%, 57%, 71%, and 83%, respectively. The

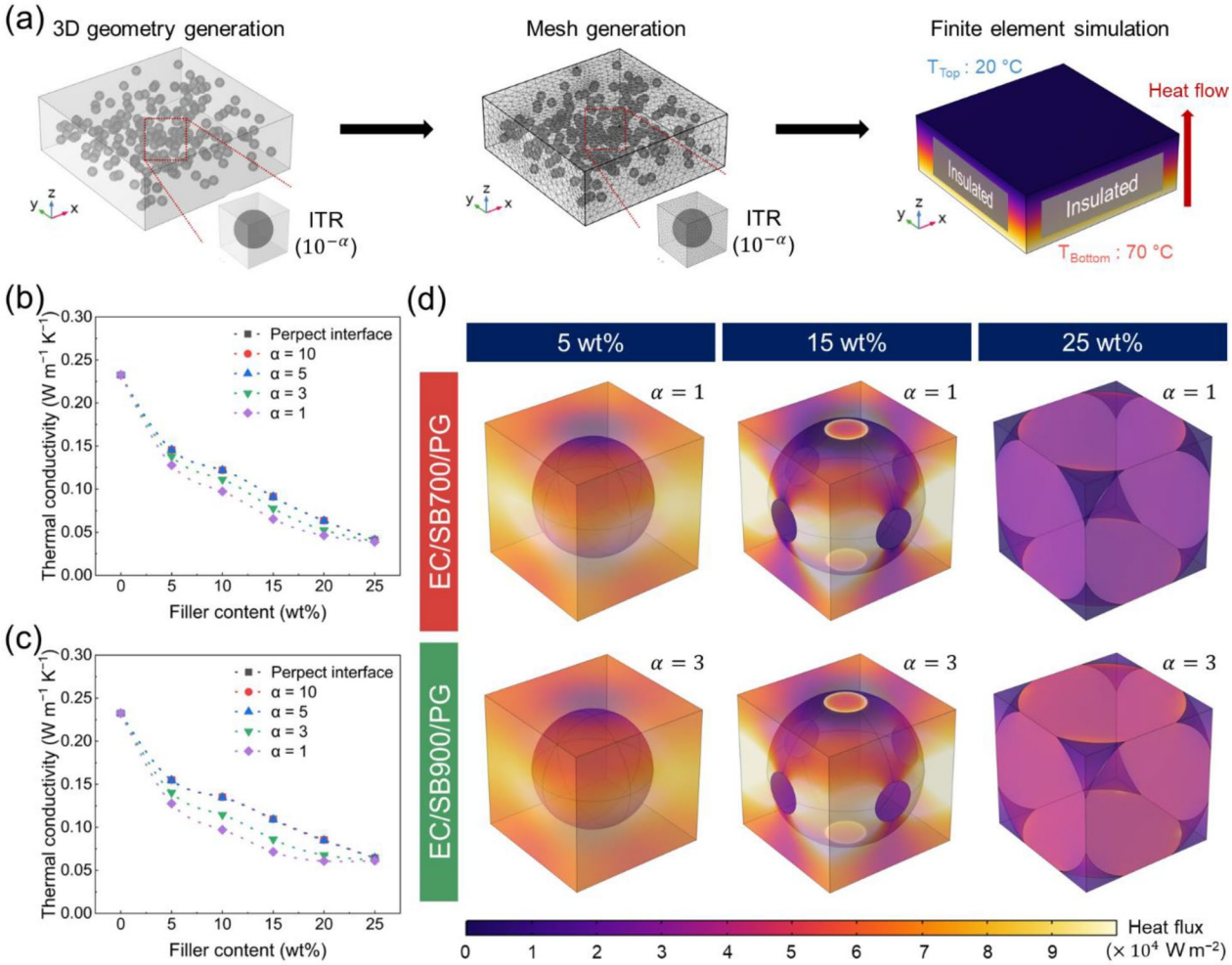

Fig. 2 FEM heat transfer analysis of SB-based composites. **a** Schematic of the FEM simulation process of SB-based composites. Effect of α on the simulated thermal conductivities of **b** SB700- and **c** SB900-based composites. **d** Heat flux distribution of SB-based composites

total porosity of SB was superior to that of SCG and enhanced at higher carbonization temperatures, while SB carbonized above 700 °C exhibited a similar level of macroporosity. The effect of carbonization temperature on the macroporosity of SB was insignificant at temperatures above 700 °C. The macropore size distribution of SB was broad due to the heterogeneous composition of the biomass waste (Adam et al. 2023), as shown in Fig. S2. The nitrogen adsorption–desorption isotherms revealed a progressive development of the porous structure with increasing carbonization temperature (Fig. S3). As the carbonization temperature increased, both the specific surface area and the micro-/mesopore volume increased, indicating that the development of micro- and mesopores is dependent on the carbonization temperature (Table S2). Meanwhile, micro- and mesopores were present only in limited proportions, whereas macropores accounted for most of the total pore volume (Fig. S4). Carbonization at 700 °C was not only more energy-efficient and environmentally friendly than high-temperature incineration but also optimal for producing SB with high macroporosity.

To determine the optimal atmosphere for the fabrication of SB, the chemical and morphological structures of NSB700 and SB700 were compared (Fig. 5). Although the chemical structure of NSB700 (Fig. 5a–d) was similar to that of SB700, graphitic N observed only in SB900 appeared with high intensity. The (002) and (100) crystal planes of graphitic carbon were also observed in NSB700 (Fig. 5e), indicating the formation of an sp^2 hybridized carbon structure. The I_D/I_G ratio of NSB700 (Fig. 5f) was 14% lower than that of SB700, which implied that carbonization under a nitrogen atmosphere improved the development of the graphitic structure. NSB700 exhibited a porous structure with a total porosity of 61%, which was approximately 10% lower than SB700

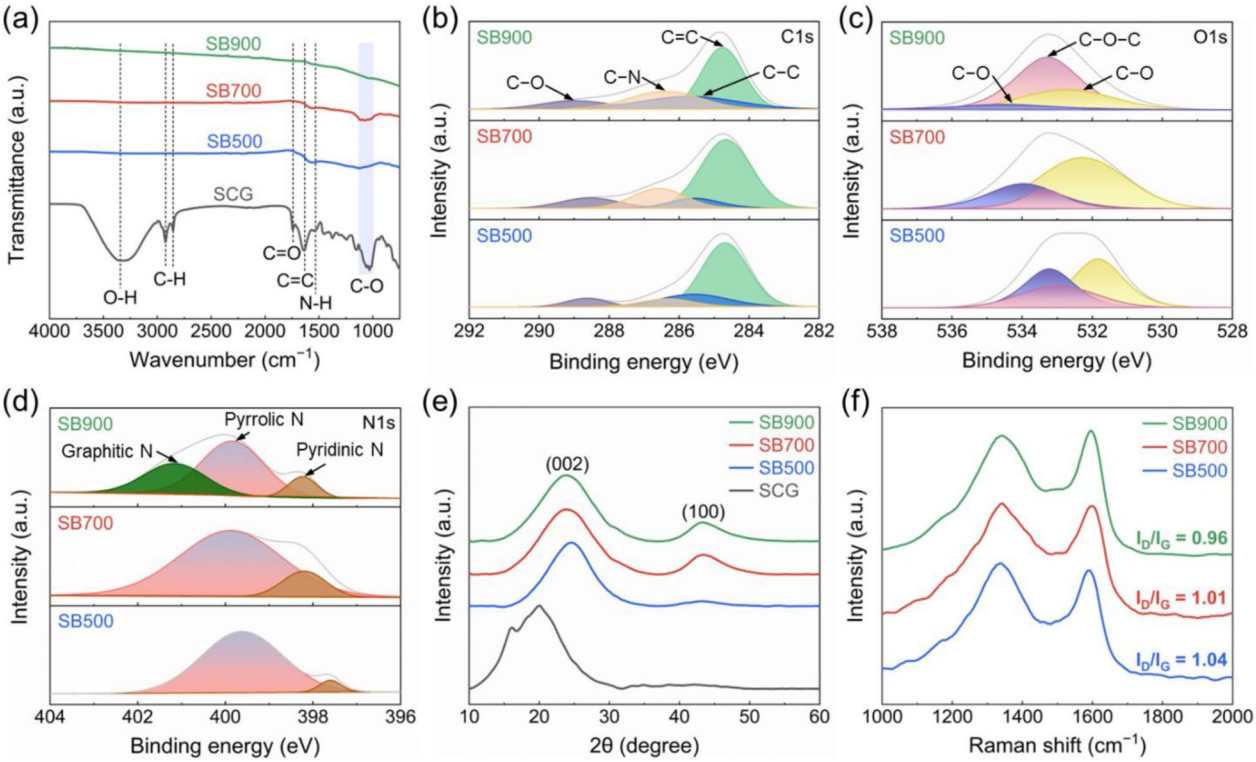

Fig. 3 Chemical characterization of SCG and as-prepared SB. **a** FT-IR spectra. Deconvoluted **b** C1s, **c** O1s, and **d** N1s XPS spectra. **e** XRD and **f** Raman spectra

(Fig. 5g–i). NSB700 showed a restricted formation of micro- and mesopores (Atinafu et al. 2025), resulting in a pore structure predominantly governed by macropores (Fig. S4). Carbonization under a nitrogen atmosphere promoted the development of graphitic carbon while simultaneously reducing porosity. As biomass undergoes pyrolysis, various gaseous byproducts are generated, with CO_2 accounting for the largest portion at approximately 60% (Yin et al. 2018). Biochar produced under an ambient atmosphere promotes surface oxidation of biomass through CO_2 released during pyrolysis and atmospheric oxygen, which together facilitate pore formation and expansion (Sun et al. 2022; Xia and Shi 2016). In contrast, continuous nitrogen flow removes gaseous byproducts and maintains an inert atmosphere, limiting the development of a porous structure. Notably, these results indicated that SB700 was more advantageous than NSB700 as a thermally insulating filler, in terms of porosity and graphitic structure.

3.2 Optimization for pore restoration

To maximize the restoration of SB pores in the composite, the solvent type and content of the pore restoration method were optimized, as shown in Fig. 6. Environmentally friendly solvents were selected based on their solubility with EC and wettability with SB. The HSP is used to determine the solubility between materials in a simple, accurate, and quantitative manner (Li et al. 2022; Kato et al. 2020). The HSP values of the materials used for thermal insulation composites are presented in Table S6. The R_a and RED were calculated using HSP to directly evaluate the solubility. (Details of the RED results are provided in Section S4.) The smaller the R_a, the stronger the solubility between the materials (Li et al. 2022; Kato et al. 2020). The R_a for EtOH was lower than that for water and PG (Fig. 6a), indicating its higher solubility in the matrix. In addition, EC has been reported to be soluble in EtOH but insoluble in water and PG (Wasilewska and Winnicka 2019). PG and EtOH exhibited low contact angles on SB (Fig. 6b), indicating excellent wettability. However, the contact angle of water with SB was the highest, resulting in low wettability. This could be attributed to the hydrophobicity induced by the carbon structure of SB (Kim et al. 2024). Therefore, SB-based composites were fabricated using three environmentally friendly solvents: (1) water, which is insoluble for EC with low wettability to SB, (2) EtOH, which is soluble for EC with good wettability to SB, and (3) PG, which is insoluble for EC but with good wettability to SB.

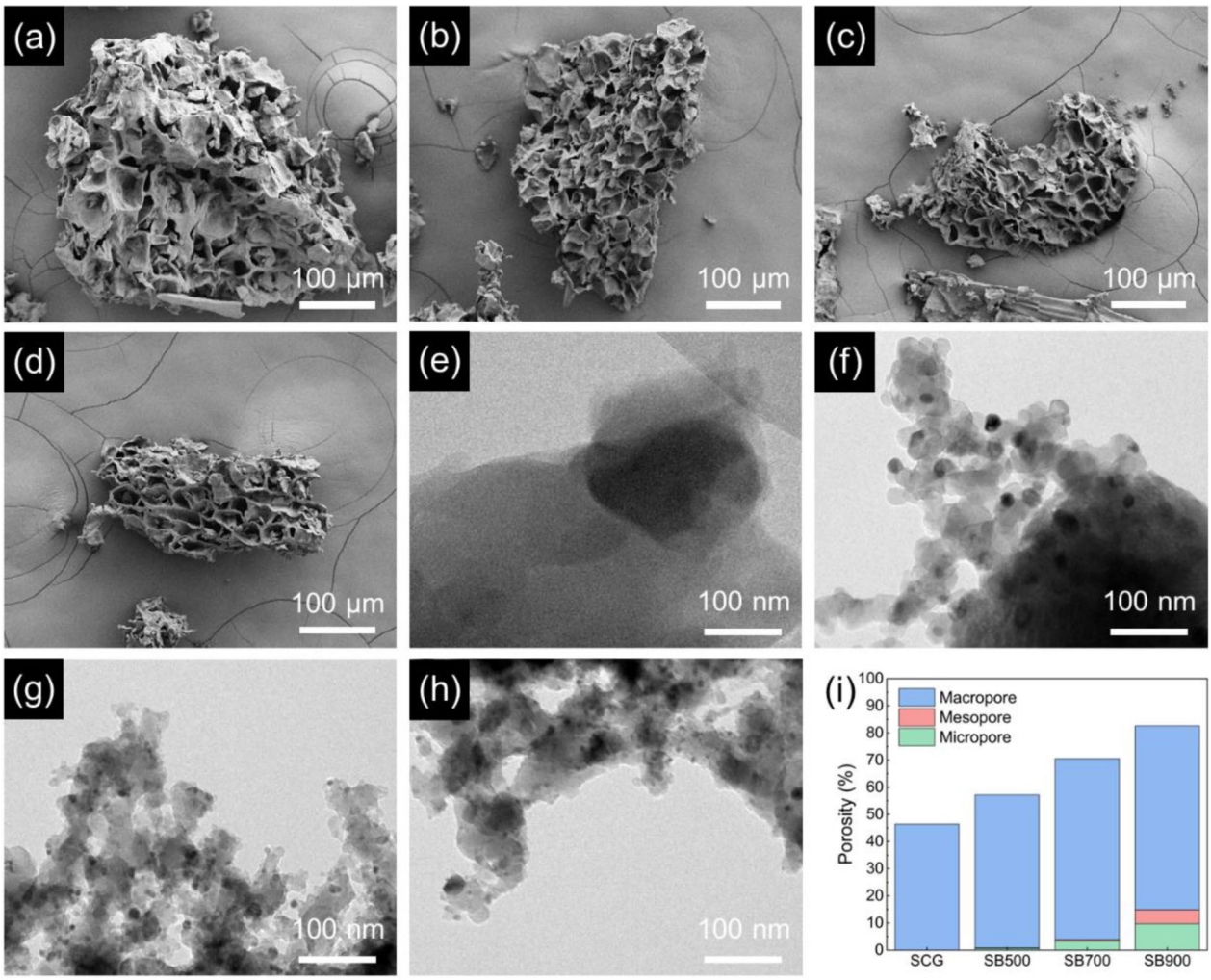

Fig. 4 Morphological characterization of SCG and as-prepared SB. FE-SEM images of **a** SCG, **b** SB500, **c** SB700, and **d** SB900. Cs-TEM images of **e** SCG, **f** SB500, **g** SB700, and **h** SB900. **i** Total porosity of SCG and SB

In Fig. 6c–j, the fracture surfaces and thermal conductivities of composites fabricated with different solvent types and content were examined to identify the optimal conditions for pore restoration. The composite without a solvent exhibited SB pores impregnated with EC. EC/SB700/water-25 and EC/SB700/none-25 exhibited similar impregnation behaviors (Fig. 6c, d). It was difficult for water to penetrate the SB pores due to its low wettability to SB, making pore restoration ineffective. The SB pores in EC/SB700/EtOH-25 were partially restored and impregnated with the dissolved EC due to the interaction of EtOH with EC and SB (Fig. 6e). EC/SB700/PG-25 exhibited well-restored pores, without impregnation of SB pores by EC (Fig. 6f). The selective affinity of PG for SB enabled the restoration of the pores without affecting the matrix. As shown in Fig. 6i, the composites with the pore restoration exhibited lower thermal conductivity due to the restoration of the pores by the solvent, as influenced by the pore restoration effect of different solvent types. EC/SB700/PG-25 exhibited the lowest thermal conductivity owing to its effective pore restoration, as observed on its fracture surface (Fig. 6f). These results suggested that the restored pores within the composite played an important role in determining thermal conductivity and that pore restoration with PG was the most effective. To determine the optimal PG content for the pore restoration method, the effect of pore restoration according to PG content was confirmed. With increasing PG content, the restored pores became more distinct, as shown in Figs. 6f–h and S5. Moreover, the thermal conductivity of the composites fabricated with PG decreased with increasing PG content (Fig. 6j). The composite with

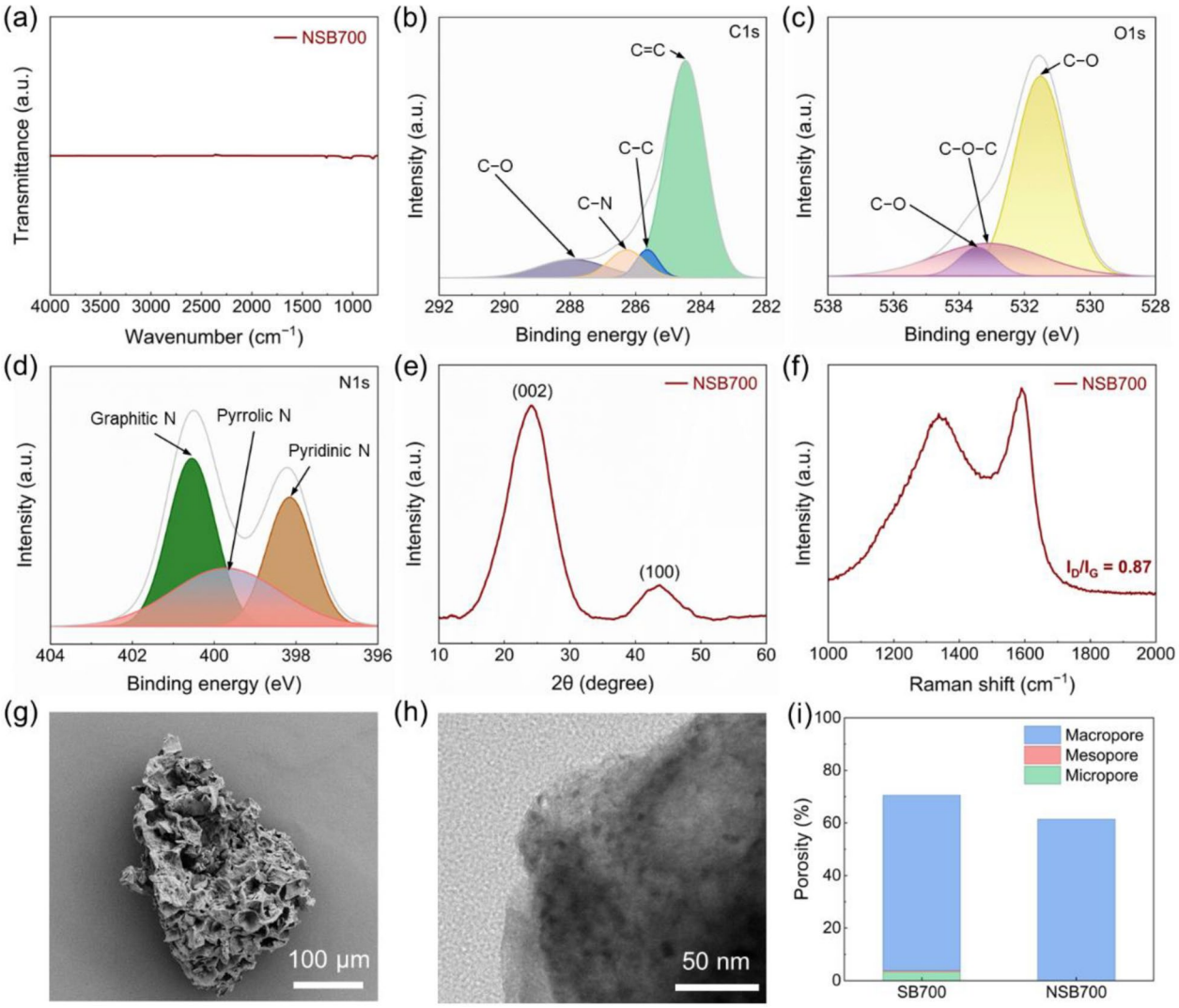

Fig. 5 Chemical and morphological characterization of NSB700. **a** FT-IR spectra. Deconvoluted **b** C1s, **c** O1s, and **d** N1s XPS spectra. **e** XRD and **f** Raman spectra. **g** FE-SEM and **h** Cs-TEM images. **i** Total porosity of NSB700 compared to SB700

PG content (2.0 g of PG per 1.0 g of SB) exhibited the highest level of pore restoration, resulting in the lowest thermal conductivity. Therefore, optimal condition (2.0 g of PG per 1.0 g of SB) was selected to fabricate SB-based thermal insulation composites with the pore restoration.

3.3 Structure of EC/SB/PG composites

To identify the restored pores in composites fabricated under the optimized condition of the pore restoration method, FE-SEM images of the fracture surfaces were observed (Figs. 6f and 7a–h). The SB pores were maintained in the composites applied with the pore restoration method, regardless of the type and content of the filler. The morphology of SB was similarly observed as confirmed in Figs. 4a–d and 5g. The porous structure was more evident in SB with higher porosity. However, FE-SEM fracture surface images could only identify the local area in the fabricated composite, making it difficult to observe the restored pore over a wider area. Consequently, a 3D non-destructive internal structural analysis using micro-CT was conducted to visualize the restored pores in 3D (Figs. 7i–p and S6 and Supplementary Video 1). The overlap between the filler area (colored) and the pore area (white) indicated that the pores of SB were restored, regardless of the type and content of the filler. These results suggested that the pore restoration method with PG effectively prevented EC impregnation into the SB pores during composite fabrication.

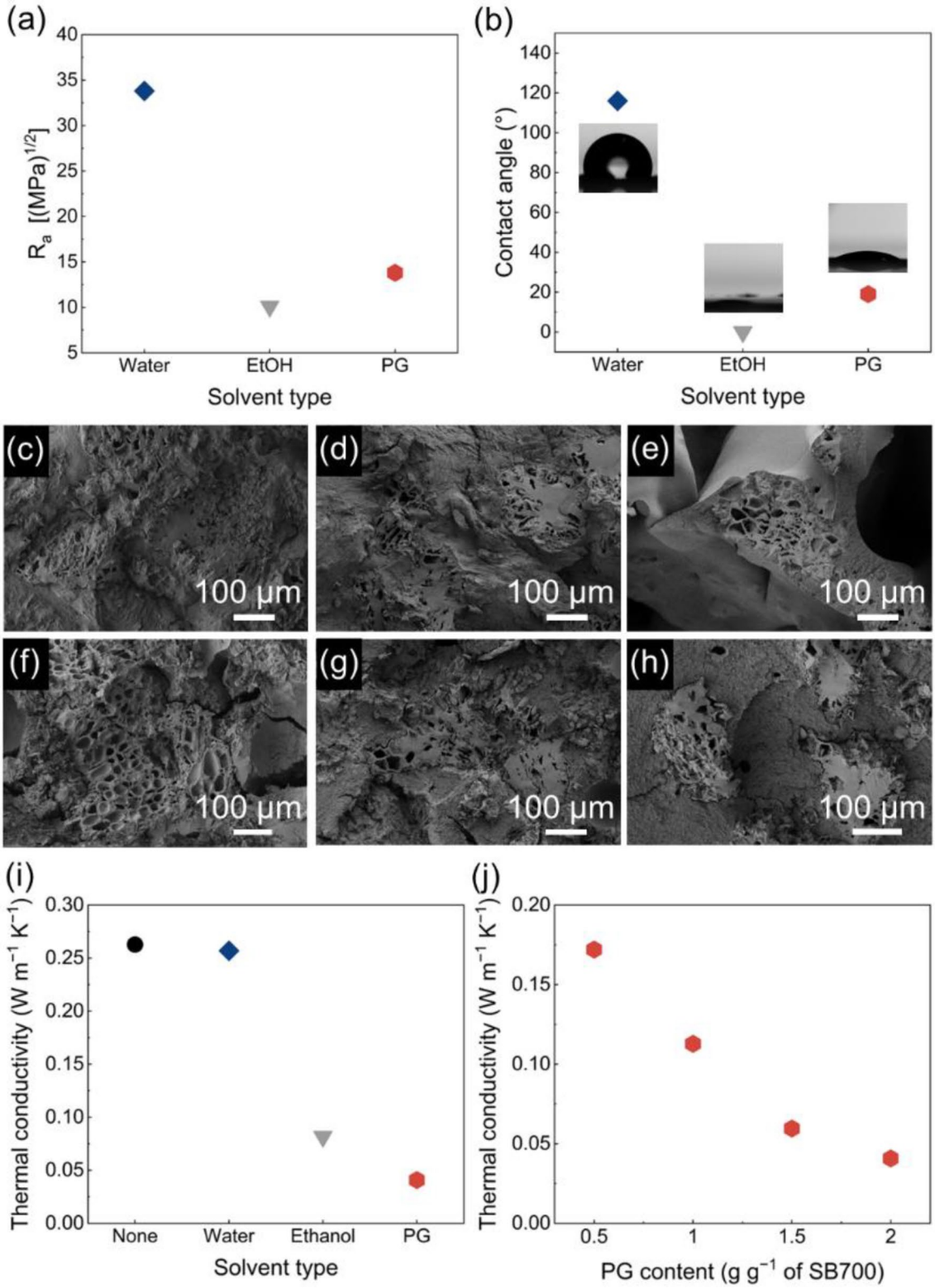

Fig. 6 Optimization of solvent type and content for the pore restoration. **a** R_a value and **b** contact angle of solvents with SB700. FE-SEM fracture surface images of SB700-based composites (25 wt%) fabricated with **c** no solvent, **d** 2.0 g of water per 1.0 g of SB700, **e** 2.0 g of EtOH per 1.0 g of SB700, **f** 2.0 g of PG per 1.0 g of SB700, **g** 1.0 g of PG per 1.0 g of SB700, and **h** 0.5 g of PG per 1.0 g of SB700. Thermal conductivity of SB700-based composites (25 wt%) fabricated with different **i** solvent types (2.0 g of solvent per 1.0 g of SB700) and **j** PG content

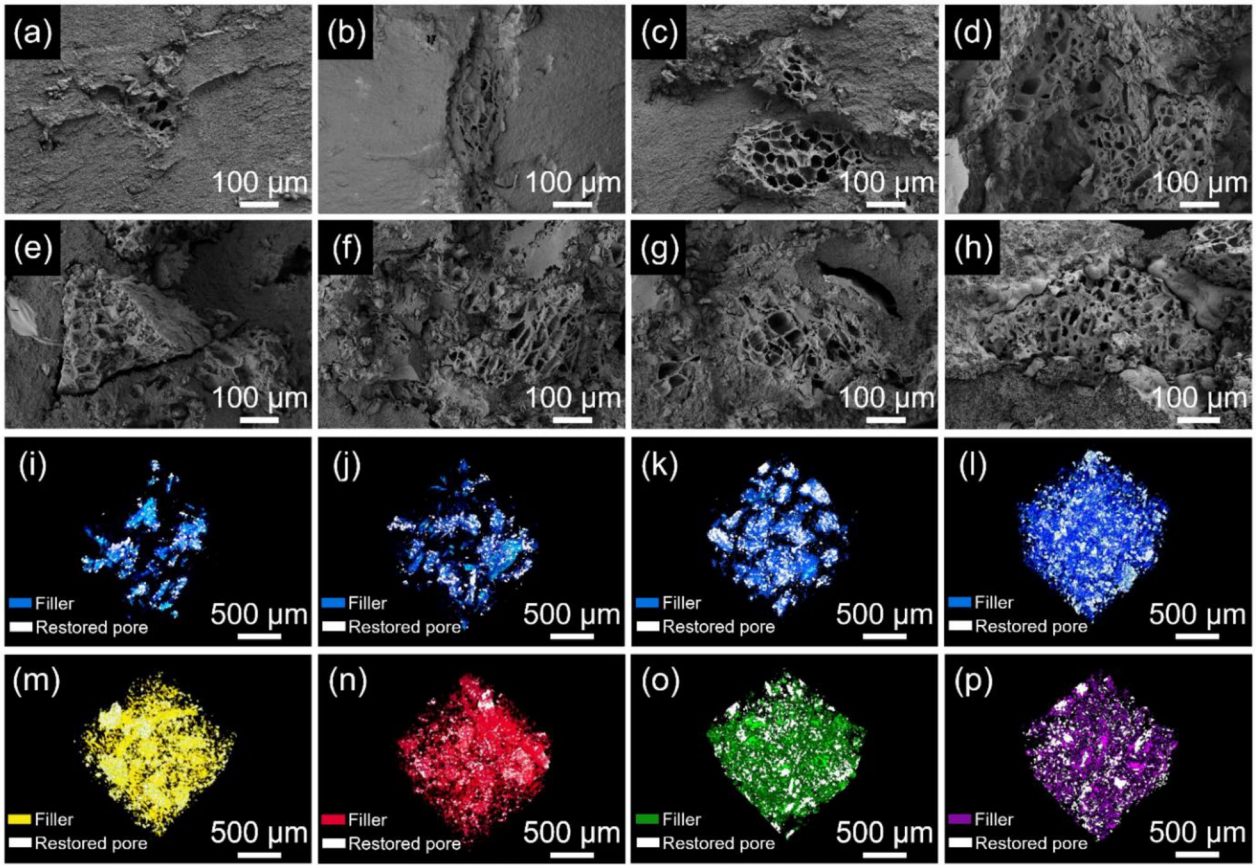

Fig. 7 Morphological characterization of composites fabricated with optimized pore restoration method. FE-SEM fracture surface images of **a** EC/SB700/PG-5, **b** EC/SB700/PG-10, **c** EC/SB700/PG-15, **d** EC/SB700/PG-20, **e** EC/SCG/PG-25, **f** EC/SB500/PG-25, **g** EC/SB900/PG-25, and **h** EC/NSB700/PG-25. Micro-CT images of **i** EC/SB700/PG-5, **j** EC/SB700/PG-10, **k** EC/SB700/PG-15, **l** EC/SB700/PG-25, **m** EC/SCG/PG-25, **n** EC/SB500/PG-25, **o** EC/SB900/PG-25, and **p** EC/NSB700/PG-25

3.4 Thermal insulation properties of EC/SB/PG composites

The thermal insulation properties of the EC/SB/PG composites are presented in Fig. 8. The SB-based composites exhibited lower thermal conductivity than the SCG-based composites (Fig. 8a). As the filler content increased, the thermal conductivity of the composites decreased gradually regardless of filler type. The composite with SB700 demonstrated the lowest thermal conductivity, and EC/SB900/PG exhibited an intermediate value between EC/SB700/PG and EC/SB500/PG. SB exhibited higher porosity than SCG, with the macroporosity of SB700 being comparable to that of SB900 and approximately 11% higher than that of SB500 (Fig. 4i). Micro- and mesoporosity of SB increased at elevated carbonization temperatures. The low thermal conductivity of the SB-based composites was ascribed to the porous structure of SB. The restored SB pores in the composite confined a significant amount of air with ultra-low thermal conductivity (0.03 W m^{-1} K^{-1}), hindering heat transfer (Zhang et al. 2023; Lee et al. 2019). Despite SB900 exhibiting comparable macropore levels and even more developed micro-/mesopores than SB700, EC/SB900/PG showed higher thermal conductivity than EC/SB700/PG. This result was attributed to the well-developed graphitic structures in SB. The graphitic structure with fewer defects minimized phonon scattering, enabling efficient heat transfer (Feng et al. 2016). The limited fraction of micro-/mesopores in SB900 is insufficient to counteract the thermal conductivity enhancement induced by its graphitic structure (Fig. S4). In addition, EC/NSB700/PG-25 exhibited a thermal conductivity that was about 4 times higher than that of EC/SB700/PG-25. This was also explained by the less developed pore structures and the more highly developed graphitic structure of NSB700 compared to SB700. Therefore, the highly porous structure of SB was advantageous for its thermal insulation properties, whereas the development of the graphitic structure increased thermal conductivity, leading to an adverse effect. Figure 8b illustrates the thermal conduction mechanism of SB-based composites, which is

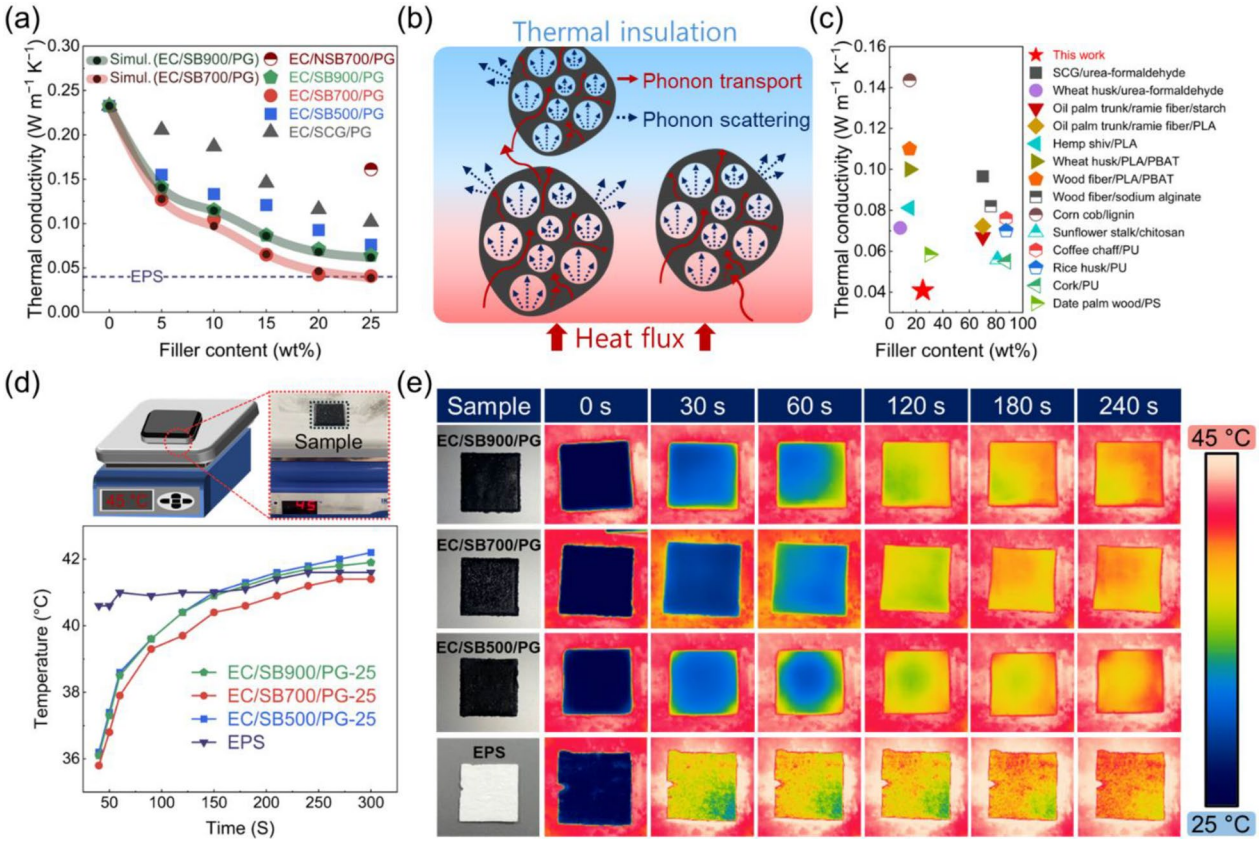

Fig. 8 Thermal insulation properties of EC/SB/PG composites. **a** Thermal conductivity and **b** heat transfer mechanism of the EC/SB/PG composites. **c** Comparison of thermal conductivity of EC/SB700/PG-25 with previously reported biomass-based thermal insulation polymer composites (Note: PLA, PBAT, and PS indicate poly(lactic acid), poly(butylene adipate-co-terephthalate), and polystyrene, respectively). **d** Temperature versus time curves and **e** thermal IR images of EC/SB/PG-25 composites

determined by the porous and graphitic structure of SB, contributing to thermal insulation performance. The thermal conductivity of EC/SB700/PG-25 was 0.04 W m^{-1} K^{-1} and exhibited about one-sixth of the thermal conductivity of EC (0.24 W m^{-1} K^{-1}), and comparable to that of EPS (0.04 W m^{-1} K^{-1}) (Dixit et al. 2019). In general, materials with a thermal conductivity below 0.07 W m^{-1} K^{-1} are regarded as thermally insulating materials (Zhang et al. 2023). Therefore, EC/SB700/PG-25 met the requirements as a thermal insulation material and outperformed previously reported biomass-based thermal insulation composites in terms of thermal conductivity (Fig. 8c) (Choi et al. 2022; Hýsek et al. 2018; Mawardi et al. 2021, 2022; Viel et al. 2019; Muthuraj et al. 2019; Lacoste et al. 2018; Mati-Baouche et al. 2014; Buratti et al. 2018; AlMallahi et al. 2024). Consequently, SB700 prepared by carbonization in an ambient atmosphere was the optimal filler that could both maximize porosity and achieve a moderately developed graphitic structure.

An FEM simulation was conducted to understand the heat transfer mechanism of SB-based composites. Since obtaining the model parameter for the simulation experimentally was challenging, α was estimated by comparing the simulated thermal conductivity with experimental data. When a perfect interface between a matrix and a filler was assumed, the simulated thermal conductivities of composites using SB700 and SB900 demonstrated a discrepancy with the experimental thermal conductivity. The fitted α values for the composites with SB700 and SB900 were $\alpha = 1$ and $\alpha = 3$, respectively, and varied depending on the filler type. As shown in Fig. 8a, the FEM simulation results were in good agreement with the experimental data when the fitted α values were applied. A low α value signified a high ITR between the filler and the matrix. Within the fabricated composite, the filler exhibited a broad pore size distribution and interfaces between dissimilar materials, which induced phonon scattering and increased ITR (Lee et al. 2019; Cho et al. 2019; Qiu et al. 2018). These results indicated that the

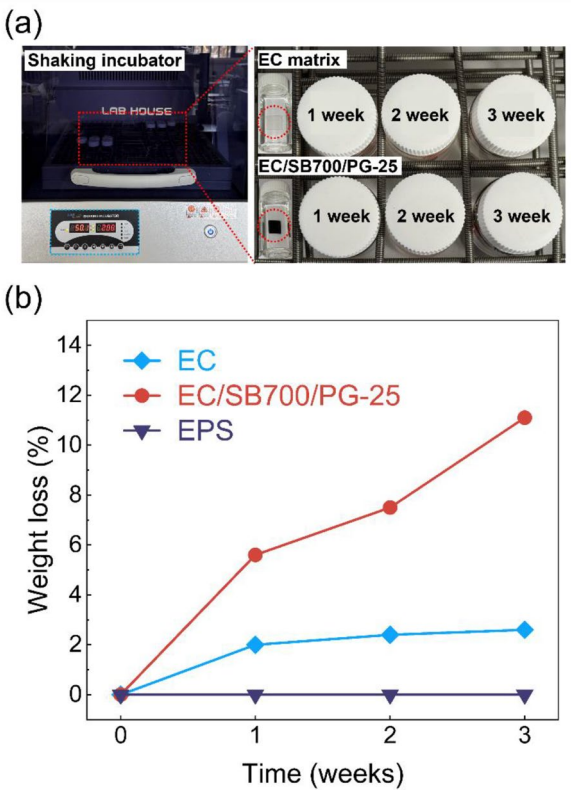

Fig. 9 Biodegradability test using cellulase enzyme. **a** Digital images of the experimental setup for the biodegradability test. **b** Weight loss of EC, EC/SB700/PG-25, and EPS during the degradation process

thermal conductivity of the SB-based composites was influenced not solely by the thermal conductivity of the filler but also by the pore structure of the highly porous SB. This intricate pore arrangement of SB enhanced the ITR between the SB and the EC matrix, impeding heat flow and consequently reducing thermal conductivity. Nonetheless, a high α value was observed in SB900, which was the result of the enhanced phonon transport due to its well-developed graphitic structure. Therefore, it was confirmed that the thermal conductivity of SB-based composites was determined by the porous and graphitic structures of SB, as well as the ITR associated with its structure.

To confirm the thermal insulation performance, thermal IR images of SB-based composites and EPS were evaluated (Fig. 8d, e). The temperature profiles of 2 mm samples using a heat source of 45 °C were observed. The temperature of commercial EPS increased rapidly to the saturation temperature of 41.6 °C due to its thin thickness. EC/SB700/PG-25 exhibited the lowest saturation temperature of 41.3 °C and the highest thermal insulation performance. The thermal insulation performance of the composites was consistent with the trend of the experimental thermal conductivity, confirming that lower thermal conductivity resulted in superior performance. Therefore, EC/SB700/PG-25 demonstrated promising potential as an environmentally friendly and viable alternative to petroleum-based thermal insulation materials.

3.5 Biodegradability of EC/SB/PG composites

The weight loss of the composite during enzymatic degradation can serve as an indicator of biodegradability (She et al. 2019). As illustrated in Fig. 9a, the experimental setup for cellulase-based degradation was designed to investigate the biodegradability of the SB-based thermal insulation composite. The weight loss of EC and EC/SB700/PG-25 over 3 weeks was examined (Fig. 9b). Pure EC exhibited a weight loss of 2.6% after 3 weeks, while the SB-based composite exhibited a faster degradation. Interestingly, SB-based composites revealed distinctive biodegradation behavior, suggesting the effect of SB incorporation. This might be due to the morphology of composites in which SB is incorporated as a filler. The incorporation of SB resulted in an imperfect interface between SB and the EC matrix, which facilitated both the enzyme and water penetration, thereby accelerating decomposition (She et al. 2019; Kadhim et al. 2025). In addition, an incompact interface between SB and EC was confirmed in the FE-SEM fracture surface image (Fig. 6f). These findings demonstrated that SB-based composites exhibited excellent biodegradability, suggesting their potential as an alternative to address the non-biodegradability issues of petroleum-based thermal insulation materials.

3.6 Application

Building integrated photovoltaic (BIPV) system consists of photovoltaic (PV) modules integrated into a building roof for the dual purposes of generating electricity and functioning as a building envelope (Boafo et al. 2022). A BIPV system effectively blocks heat from the solar source outside the building, providing thermal comfort (Martín-Chivelet et al. 2022). However, it also leads to an increase in building temperature due to the heat generated by the PV modules (Singh and Chaudhary 2022). To alleviate the temperature problem of the BIPV system, thermally insulating materials are required behind the PV module (Singh and Chaudhary 2022). Although conventional petroleum-based thermal insulation materials have been used in BIPV systems (Boafo et al. 2022; Singh and Chaudhary 2022), there is an urgent need to consider the environmental issues that arise during disposal. Therefore, an environmentally friendly SB-based composite was applied as a thermal insulation material to block heat generated by the PV module. As represented in Figs. 10a

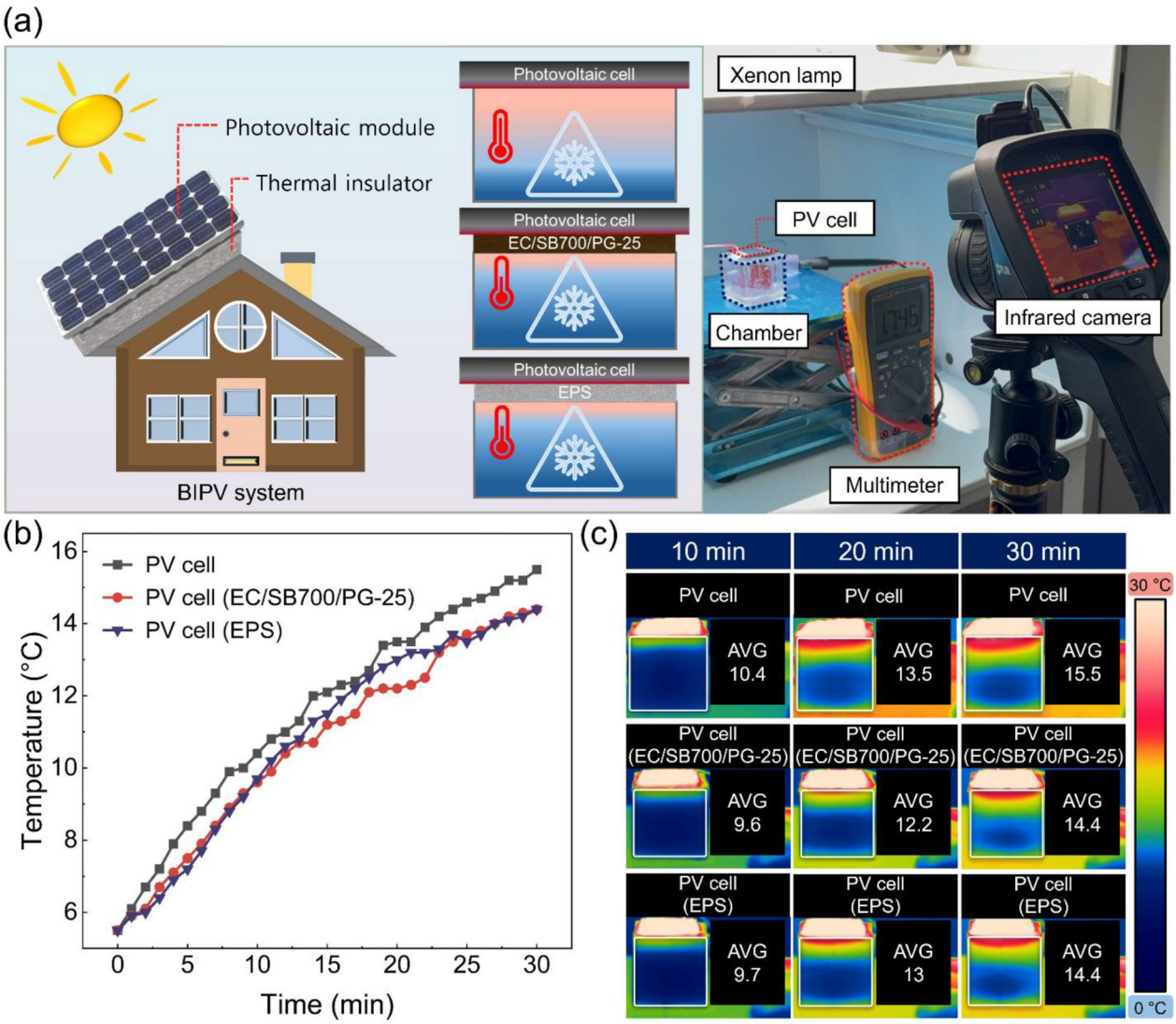

Fig. 10 Thermal insulation ability of SB-based composite in BIPV system. **a** Schematic diagram and digital image of the experimental setup in the scaled-down BIPV system. **b** Temperature versus time curve and **c** thermal IR images of the chamber during the scaled-down BIPV system experiment

and S7 and Supplementary Video 2, the experimental setup was designed to evaluate the thermal insulation performance of materials integrated into the operating PV cell. The effect of the thermally insulating material was verified based on the interior temperature profile and the state of ice in the chamber (Figs. 10b, c and S8 and Supplementary Videos 3 and 4). When the EPS and EC/SB700/PG-25 were applied to the PV cell, the temperature variations in the chamber were significantly reduced, and the change from ice to liquid was delayed. A similar temperature trend was observed in the chamber when the PV cell integrated with EPS and EC/SB700/PG-25 was applied, demonstrating comparable insulation performance against the heat generated by the PV cell. Therefore, it is suggested that integrating SB-based composite into a BIPV system could effectively regulate the heat generated from the PV modules and prevent the temperature increase inside the building. More importantly, SB-based thermal insulation materials have the potential to replace conventional petroleum-based insulation materials, not only in BIPV systems but in various fields as well.

4 Conclusion

In summary, we developed biodegradable SB-based thermal insulation composites for the first time, using SB and EC as raw materials. SB was fabricated by a simple carbonization process of SCG, and the chemical and morphological properties of SB were significantly affected by carbonization temperature and atmosphere. SB700, carbonized at 700 °C in an ambient atmosphere, was the optimal filler with a porosity of 71% and a moderately developed graphitic structure. Environmentally friendly PG, used as a solvent for the pore restoration, ensured that the SB pores were not impregnated with the matrix during composite fabrication. The SB-based thermal insulation composite exhibited a low thermal conductivity of 0.04 $W\ m^{-1}\ K^{-1}$, which is superior to that of biomass-based thermal insulation composites and comparable to that of commercial EPS. In addition, our work suggests that the porosity and graphitic structure of SB played a crucial role in the thermal conductivity of the SB-based thermal insulation composite. The porous and graphitic structures of SB induced phonon scattering and transport, respectively, thereby determining the thermal conduction mechanisms in SB-based composites. Furthermore, the heat transfer mechanism of SB-based composites was theoretically verified through FEM simulations. These findings demonstrate that SB-based composites with superior thermal insulation performance, sustainability, and biodegradability have great potential for practical applications in thermal insulation industries.

Supplementary Information

The online version contains supplementary material available at https://doi.org/10.1007/s42773-026-00584-1.

Additional file 1

Additional file 2

Additional file 3

Additional file 4

Additional file 5

Acknowledgements

Samples were analyzed by Cs-TEM (JEM-ARM200F, JEOL, Peabody, MA, USA) installed at the Center for University-wide Research Facilities (CURF) at Jeonbuk National University.

Author contributions

All authors contributed to the study conception and design. Material preparation, data collection, methodology, data analysis, visualization, and validation were performed by Sung Jin Kim; Conceptualization, methodology, supervision, writing-review & editing, project administration, funding acquisition were performed by Seong Yun Kim; The first draft of the manuscript was written by Sung Jin Kim and all authors commented on previous versions of the manuscript. All authors read and approved the final manuscript.

Funding

This work was supported by the Technology Innovation Program (RS-2024-00420431, Development of hydrogen storage tube skid for land and sea transportation using high-strength carbon fiber) funded by the Ministry of Trade Industry & Energy (MOTIE, Korea).

Data availability

The datasets used or analyzed during the current study are available from the corresponding author upon reasonable request.

Declarations

Competing interests

The authors have no relevant financial or non-financial interests to disclose.

Author details

[1]Department of Carbon Composites Convergence Materials Engineering, Jeonbuk National University, Jeonju 54896, Republic of Korea.

Received: 14 July 2025 Revised: 13 January 2026 Accepted: 14 January 2026
Published online: 10 March 2026

References

Abu-Jdayil B, Barkhad MS, Mourad A-HI, Iqbal MZ (2021) Date palm wood waste-based composites for green thermal insulation boards. J Build Eng 43:103224. https://doi.org/10.1016/j.jobe.2021.103224

Adam R, Pollex A, Zeng T et al (2023) Systematic homogenization of heterogenous biomass batches–industrial-scale production of solid biofuels in two case studies. Biomass Bioenerg 173:106808. https://doi.org/10.1016/j.biombioe.2023.106808

AlMallahi MN, Al Abdallah H, Abu-Jdayil B, Elgendi M (2024) Enhancing evaporation using proposed biomass-derived insulation with holistic decision-making. Appl Therm Eng 253:123662. https://doi.org/10.1016/j.applthermaleng.2024.123662

Andrade TS, Vakros J, Mantzavinos D, Lianos P (2020) Biochar obtained by carbonization of spent coffee grounds and its application in the construction of an energy storage device. Chem Eng J Adv 4:100061. https://doi.org/10.1016/j.ceja.2020.100061

Atinafu DG, Choi JY, Nam J, Kang Y, Kim S (2025) Insights into the effects of biomass feedstock and pyrolysis conditions on the energy storage capacity and durability of standard biochar-based phase-change composites. Biochar 7:18. https://doi.org/10.1007/s42773-024-00396-1

Batista MJ, Ávila AF, Franca AS, Oliveira LS (2020) Polysaccharide-rich fraction of spent coffee grounds as promising biomaterial for films fabrication. Carbohydr Polym 233:115851. https://doi.org/10.1016/j.carbpol.2020.115851

Bejenari V, Marcu A, Ipate A-M et al (2021) Physicochemical characterization and energy recovery of spent coffee grounds. J Mater Res Technol 15:4437–4451. https://doi.org/10.1016/j.jmrt.2021.10.064

Boafo FE, Kim J-H, Ahn J-G, Kim S-M, Kim J-T, Zhang L (2022) Study on thermal characteristics and electrical performance of a hybrid building integrated photovoltaic (BIPV) system combined with vacuum insulation panel (VIP). Energy Build 277:112574. https://doi.org/10.1016/j.enbuild.2022.112574

Boonrawd C, Yodyingyong S, Benyahia L, Triampo D (2022) Novel solvent–latex mixing: thermal insulation performance of silica aerogel/natural rubber composite. Gels 8(1):7. https://doi.org/10.3390/gels8010007

Brown KR, Xue Z, Cordier R et al (2024) 1, 4-cineole: a bio-derived solvent for highly stable graphene nanoplatelet suspensions and well-dispersed UHMWPE nanocomposite fibers. Adv Compos Hybrid Mater 7(5):160. https://doi.org/10.1007/s42114-024-00977-5

Buratti C, Belloni E, Lascaro E, Merli F, Ricciardi P (2018) Rice husk panels for building applications: thermal, acoustic and environmental characterization and comparison with other innovative recycled waste materials. Constr Build Mater 171:338–349. https://doi.org/10.1016/j.conbuildmat.2018.03.089

Chan H, Shi C, Wu Z et al (2022) Superhydrophilic three-dimensional porous spent coffee ground reduced palladium nanoparticles for efficient

catalytic reduction. J Colloid Interface Sci 608:1414–1421. https://doi.org/10.1016/j.jcis.2021.10.028
Chen C, Zhou Y, Xie W et al (2023) Lightweight, thermally insulating, fire-proof graphite-cellulose foam. Adv Funct Mater 33(6):2204219. https://doi.org/10.1002/adfm.202204219
Cho J, Jang HG, Kim SY, Yang B (2019) Flexible and coatable insulating silica aerogel/polyurethane composites via soft segment control. Compos Sci Technol 171:244–251. https://doi.org/10.1016/j.compscitech.2018.12.027
Choi JY, Yun BY, Kim YU, Kang Y, Lee SC, Kim S (2022) Evaluation of thermal/acoustic performance to confirm the possibility of coffee waste in building materials in using bio-based microencapsulated PCM. Environ Pollut 294:118616. https://doi.org/10.1016/j.envpol.2021.118616
De Rosa M, Bianco V (2023) Optimal insulation layer for heated water pipes under technical, economic and carbon emission constraints. Energy 270:126961. https://doi.org/10.1016/j.energy.2023.126961
Dell'Orso M, Mangialardi T, Paolini AE, Piga L (2012) Evaluation of the leachability of heavy metals from cement-based materials. J Hazard Mater 227–228:1–8. https://doi.org/10.1016/j.jhazmat.2012.04.017
Desole MP, Gisario A, Fedele L, Aversa C, Barletta M (2024) Life cycle assessment of secondary packaging. expanded polystyrene versus bioplastic-coated corrugated cardboard. Sustain Prod Consum 46:11–28. https://doi.org/10.1016/j.spc.2024.02.010
Di Canto JAT, Malfait WJ, Wernery J (2023) Turning waste into insulation—a new sustainable thermal insulation board based on wheat bran and banana peels. Build Environ 244:110740. https://doi.org/10.1016/j.buildenv.2023.110740
Dixit A, Dai Pang S, Kang S-H, Moon J (2019) Lightweight structural cement composites with expanded polystyrene (EPS) for enhanced thermal insulation. Cem Concr Compos 102:185–197. https://doi.org/10.1016/j.cemconcomp.2019.04.023
Feng W, Qin M, Feng Y (2016) Toward highly thermally conductive all-carbon composites: structure control. Carbon 109:575–597. https://doi.org/10.1016/j.carbon.2016.08.059
García-García D, Carbonell A, Samper M, García-Sanoguera D, Balart R (2015) Green composites based on polypropylene matrix and hydrophobized spend coffee ground (SCG) powder. Compos Part B Eng 78:256–265. https://doi.org/10.1016/j.compositesb.2015.03.080
Ghorbani M, Konvalina P, Neugschwandtner RW et al (2024) How do different feedstocks and pyrolysis conditions effectively change biochar modification scenarios? A critical analysis of engineered biochars under H2O2 oxidation. Energy Convers Manag 300:117924. https://doi.org/10.1016/j.enconman.2023.117924
Hansen CM (1967) The three dimensional solubility parameter. Danish Technical: Copenhagen 14
Hýsek Š, Podlena M, Bartsch H, Wenderdel C, Böhm M (2018) Effect of wheat husk surface pre-treatment on the properties of husk-based composite materials. Ind Crops Prod 125:105–113. https://doi.org/10.1016/j.indcrop.2018.08.035
Kadhim MA, Yan X, Han R et al (2025) High-performance biodegradable dielectric composite: towards minimizing electronic waste. Compos Part A Appl Sci Manuf 188:108583. https://doi.org/10.1016/j.compositesa.2024.108583
Kataya G, Cornu D, Bechelany M, Hijazi A, Issa M (2023) Biomass waste conversion technologies and its application for sustainable environmental development—a review. Agronomy 13(11):2833. https://doi.org/10.3390/agronomy13112833
Kato Y, Osawa T, Yoshihara M, Fujii H, Tsutsumi S, Yamamoto H (2020) Evaluation of the antifoaming effect using Hansen solubility parameters. ACS Omega 5(11):5684–5690. https://doi.org/10.1021/acsomega.9b03567
Kim HM, Noh YJ, Yu J, Kim SY, Youn JR (2015) Silica aerogel/polyvinyl alcohol (PVA) insulation composites with preserved aerogel pores using interfaces between the superhydrophobic aerogel and hydrophilic PVA solution. Compos Part A Appl Sci Manuf 75:39–45. https://doi.org/10.1016/j.compositesa.2015.04.014
Kim Y-G, Kim HS, Jo SM et al (2018) Thermally insulating, fire-retardant, smokeless and flexible polyvinylidene fluoride nanofibers filled with silica aerogels. Chem Eng J 351:473–481. https://doi.org/10.1016/j.cej.2018.06.102
Kim M-J, Choi SW, Kim H, Mun S, Lee KB (2020) Simple synthesis of spent coffee ground-based microporous carbons using K2CO3 as an activation agent and their application to CO2 capture. Chem Eng J 397:125404. https://doi.org/10.1016/j.cej.2020.125404
Kim SJ, Nam HE, Lee H, Kim SH, Jang J-u, Kim SY (2024) Ethyl cellulose/carbonized spent coffee ground-based biocomposites for superior hydrophobicity and electric protection performance. Compos Part A Appl Sci Manuf 177:107964. https://doi.org/10.1016/j.compositesa.2023.107964
Kim J, Lee J, Lee S, Kwon O, Lee J, Kim J (2025) Enhanced biodegradability and thermal insulation capability of polylactic acid reinforced with calcium-crosslinked orange peel biochar. Ind Crops Prod 226:120666. https://doi.org/10.1016/j.indcrop.2025.120666
Lachheb A, Allouhi A, El Marhoune M et al (2019) Thermal insulation improvement in construction materials by adding spent coffee grounds: an experimental and simulation study. J Clean Prod 209:1411–1419. https://doi.org/10.1016/j.jclepro.2018.11.140
Lacoste C, El Hage R, Bergeret A, Corn S, Lacroix P (2018) Sodium alginate adhesives as binders in wood fibers/textile waste fibers biocomposites for building insulation. Carbohydr Polym 184:1–8. https://doi.org/10.1016/j.carbpol.2017.12.019
Lee H, Lee D, Cho J et al (2019) Super-insulating, flame-retardant, and flexible poly (dimethylsiloxane) composites based on silica aerogel. Compos Part A Appl Sci Manuf 123:108–113. https://doi.org/10.1016/j.compositesa.2019.05.004
Lee K-T, Cheng C-L, Lee D-S et al (2022) Spent coffee grounds biochar from torrefaction as a potential adsorbent for spilled diesel oil recovery and as an alternative fuel. Energy 239:122467. https://doi.org/10.1016/j.energy.2021.122467
Li M, Ren T, Sun Y et al (2022) New parameter derived from the hansen solubility parameter used to evaluate the solubility of asphaltene in solvent. ACS Omega 7(16):13801–13807. https://doi.org/10.1021/acsomega.2c00018
Li W, Yan D, Li L et al (2023) Review of thermal treatments for the degradation of dioxins in municipal solid waste incineration fly ash: proposing a suitable method for large-scale processing. Sci Total Environ 875:162565. https://doi.org/10.1016/j.scitotenv.2023.162565
Li B, Li J, Guo M (2024) Preparation of low internal resistance electrode material with multistage interconnected pores from coffee grounds. Adv Compos Hybrid Mater 7(2):48. https://doi.org/10.1007/s42114-024-00858-x
Liu S-H, Huang Y-Y (2018) Valorization of coffee grounds to biochar-derived adsorbents for CO2 adsorption. J Clean Prod 175:354–360. https://doi.org/10.1016/j.jclepro.2017.12.076
MacLeod M, Arp HPH, Tekman MB, Jahnke A (2021) The global threat from plastic pollution. Science 373(6550):61–65. https://doi.org/10.1126/science.abg5433
Martín-Chivelet N, Kapsis K, Wilson HR et al (2022) Building-integrated photovoltaic (BIPV) products and systems: a review of energy-related behavior. Energy Build 262:111998. https://doi.org/10.1016/j.enbuild.2022.111998
Martinez CLM, Saari J, Melo Y, Cardoso M, de Almeida GM, Vakkilainen E (2021) Evaluation of thermochemical routes for the valorization of solid coffee residues to produce biofuels: a Brazilian case. Renew Sustain Energy Rev 137:110585. https://doi.org/10.1016/j.rser.2020.110585
Mati-Baouche N, De Baynast H, Lebert A et al (2014) Mechanical, thermal and acoustical characterizations of an insulating bio-based composite made from sunflower stalks particles and chitosan. Ind Crops Prod 58:244–250. https://doi.org/10.1016/j.indcrop.2014.04.022
Mawardi I, Aprilia S, Faisal M, Rizal S (2021) Characterization of thermal bio-insulation materials based on oil palm wood: the effect of hybridization and particle size. Polymers 13(19):3287. https://doi.org/10.3390/polym13193287
Mawardi I, Aprilia S, Faisal M, Rizal S (2022) Investigation of thermal conductivity and physical properties of oil palm trunks/ramie fiber reinforced biopolymer hybrid composites as building bio-insulation. Mater Today Proc 60:373–377. https://doi.org/10.1016/j.matpr.2022.01.249
McNutt J, He QS (2019) Spent coffee grounds: a review on current utilization. J Ind Eng Chem 71:78–88. https://doi.org/10.1016/j.jiec.2018.11.054
Mengesha DN, Abebe MW, Appiah-Ntiamoah R, Kim H (2022) Ground coffee waste-derived carbon for adsorptive removal of caffeine: effect of surface chemistry and porous structure. Sci Total Environ 818:151669. https://doi.org/10.1016/j.scitotenv.2021.151669
Mort R, Vorst K, Curtzwiler G, Jiang S (2021) Biobased foams for thermal insulation: material selection, processing, modelling, and performance. RSC Adv 11(8):4375–4394. https://doi.org/10.1039/D0RA09287H
Muthuraj R, Lacoste C, Lacroix P, Bergeret A (2019) Sustainable thermal insulation biocomposites from rice husk, wheat husk, wood fibers and textile

waste fibers: elaboration and performances evaluation. Ind Crops Prod 135:238–245. https://doi.org/10.1016/j.indcrop.2019.04.053
Oh W-D, Veksha A, Chen X et al (2019) Catalytically active nitrogen-doped porous carbon derived from biowastes for organics removal via peroxymonosulfate activation. Chem Eng J 374:947–957. https://doi.org/10.1016/j.cej.2019.06.001
Oprea M, Voicu SI (2020) Recent advances in composites based on cellulose derivatives for biomedical applications. Carbohydr Polym 247:116683. https://doi.org/10.1016/j.carbpol.2020.116683
Park JH, Kim YU, Jeon J, Yun BY, Kang Y, Kim S (2021) Analysis of biochar-mortar composite as a humidity control material to improve the building energy and hygrothermal performance. Sci Total Environ 775:145552. https://doi.org/10.1016/j.scitotenv.2021.145552
Qi Y, Xue X, Dong X et al (2024) Ameliorating the comprehensive performance of rigid polyurethane foam insulating materials by green cork for building energy conservation. Compos Commun 52:102132. https://doi.org/10.1016/j.coco.2024.102132
Qiu L, Zou H, Tang D, Wen D, Feng Y, Zhang X (2018) Inhomogeneity in pore size appreciably lowering thermal conductivity for porous thermal insulators. Appl Therm Eng 130:1004–1011. https://doi.org/10.1016/j.applthermaleng.2017.11.066
Rodier L, Bilba K, Onésippe C, Arsène M-A (2019) Utilization of bio-chars from sugarcane bagasse pyrolysis in cement-based composites. Ind Crops Prod 141:111731. https://doi.org/10.1016/j.indcrop.2019.111731
Seo J, Kearney LT, Toomey MD, Keum JK, Naskar AK (2023) Polyester-based epoxy vitrimer integrating spent coffee ground as a natural filler. Compos Part B Eng 260:110756. https://doi.org/10.1016/j.compositesb.2023.110756
Shakeel F, Haq N, Alanazi FK, Alsarra IA (2014) Measurement and correlation of solubility of olmesartan medoxomil in six green solvents at 295.15–330.15 K. Ind Eng Chem Res 53(7):2846–2849. https://doi.org/10.1021/ie404373n
She D, Dong J, Zhang J et al (2019) Development of black and biodegradable biochar/gutta percha composite films with high stretchability and barrier properties. Compos Sci Technol 175:1–5. https://doi.org/10.1016/j.compscitech.2019.03.007
Shi C, Zhang X, Nilghaz A et al (2023) Large-scale production of spent coffee ground-based photothermal materials for high-efficiency solar-driven interfacial evaporation. Chem Eng J 455:140361. https://doi.org/10.1016/j.cej.2022.140361
Singh D, Chaudhary R (2022) Performance evaluation of thermally insulated building integrated photovoltaic roof. Mater Today Proc 52:888–892. https://doi.org/10.1016/j.matpr.2021.10.294
Sun Z, Dai L, Lai P, Shen F, Shen F, Zhu W (2022) Air oxidation in surface engineering of biochar-based materials: a critical review. Carbon Res 1:32. https://doi.org/10.1007/s44246-022-00031-3
Tan Z, Yoo CG, Yang D, Liu W, Qiu X, Zheng D (2023) "Rigid-Flexible" anisotropic biomass-derived aerogels with superior mechanical properties for oil recovery and thermal insulation. ACS Appl Mater Interfaces 15(35):42080–42903. https://doi.org/10.1021/acsami.3c07713
Varamesh A, Zhu Y, Hu G et al (2024) Fully biobased thermal insulating aerogels with superior fire-retardant and mechanical properties. Chem Eng J 495:153587. https://doi.org/10.1016/j.cej.2024.153587
Viel M, Collet F, Lanos C (2019) Development and characterization of thermal insulation materials from renewable resources. Constr Build Mater 214:685–697. https://doi.org/10.1016/j.conbuildmat.2019.04.139
Wan Z, Sun Y, Tsang DC et al (2020) Customised fabrication of nitrogen-doped biochar for environmental and energy applications. Chem Eng J 401:126136. https://doi.org/10.1016/j.cej.2020.126136
Wasilewska K, Winnicka K (2019) Ethylcellulose–a pharmaceutical excipient with multidirectional application in drug dosage forms development. Materials 12(20):3386. https://doi.org/10.3390/ma12203386
Woo D-G, Kim SH, Kim TH (2021) Solid fuel characteristics of pellets comprising spent coffee grounds and wood powder. Energies 14(2):371. https://doi.org/10.3390/en14020371
Xia C, Shi QS (2016) Self-activation for activated carbon from biomass: theory and parameters. Green Chem 18:2063. https://doi.org/10.1039/C5GC02152A
Xu Q, Townsend T, Bitton G (2011) Inhibition of hydrogen sulfide generation from disposed gypsum drywall using chemical inhibitors. J Hazard Mater 191:204–211. https://doi.org/10.1016/j.jhazmat.2011.04.063
Xu X, Hu R, Chen M et al (2020) 3D boron nitride foam filled epoxy composites with significantly enhanced thermal conductivity by a facial and scalable approach. Chem Eng J 397:125447. https://doi.org/10.1016/j.cej.2020.125447
Xu C, Tong S, Sun L, Gu X (2023) Cellulase immobilization to enhance enzymatic hydrolysis of lignocellulosic biomass: an all-inclusive review. Carbohydr Polym 321:121319. https://doi.org/10.1016/j.carbpol.2023.121319
Yin Y, Gao Y, Li A (2018) Self-activation of biochar from furfural residues by recycled pyrolysis gas. Waste Manag 77:312–321. https://doi.org/10.1016/j.wasman.2018.04.014
Zhang M, Zhang Z, Zhang R, Peng Y, Wang M, Cao J (2023) Lightweight, thermal insulation, hydrophobic mycelium composites with hierarchical porous structure: design, manufacture and applications. Compos Part B Eng 266:111003. https://doi.org/10.1016/j.compositesb.2023.111003
Zhang J, Han Y, Zhang L et al (2024b) Silica aerogel-PVA dough: a high internal phase composite with superior thermal insulation and gas barrier. Compos Sci Technol 251:110553. https://doi.org/10.1016/j.compscitech.2024.110553
Zhang X, Gao Y, Wang X et al (2024a) A flexible, thermal-insulating, and fire-resistant bagasse-derived cellulose aerogel prepared via a refrigerator freezing combined ambient pressure drying technique. Chem Eng J 498:155466. https://doi.org/10.1016/j.cej.2024.155466
Zhang Y, Li M, Zhu X, Wang L, Mašek O, Sarmah AK, Tsang DCW (2025) Enhanced thermal insulation of biochar-gypsum composites. Cem Concr Compos 159:106013. https://doi.org/10.1016/j.cemconcomp.2025.106013
Zhou S, Tang Z, Pan Z et al (2022) Regulating closed pore structure enables significantly improved sodium storage for hard carbon pyrolyzing at relatively low temperature. SusMat 2(3):357–367. https://doi.org/10.1002/sus2.60